- Technical Paper -

SIMULATION OF SHRINKAGE BEHAVIORS BASED ON EARLY AGE HYDRATION AND MOISTURE STATE IN PORE STRUCTURE

Yao LUAN[*1], Tetsuya ISHIDA[*2]

ABSTRACT

A multi-scale constitutive model is improved based on early age hydration and moisture state in micro-pores. It is found that the original model underestimates autogenous shrinkage at initial days. Therefore the contribution of chemical shrinkage at early age is discussed and added. Besides, long time shrinkage is modified, considering driving forces acting on pores with different radii respectively, such as capillary tension and disjoining pressure. With the improved model, autogenous and drying shrinkage with various w/c ratios and relative humidity can be simulated reasonably.

Keywords: autogenous shrinkage, drying shrinkage, capillary tension, disjoining pressure

1. INTRODUCTION

Concrete made with low water-cement (w/c) ratio is being widely used in practice nowadays. Although low w/c ratio brings high strength and low permeability, autogenous shrinkage becomes much more significant. Tensile stress would be induced in concrete, resulting in early-age cracking and greatly decreasing the long term performance of structures.

The mechanism of autogenous shrinkage is usually regarded as similar to drying shrinkage in some extent. Due to water loss by self-desiccation or exposure, the internal relative humidity (RH) decreases and driving force occurs. Several theories have been proposed to describe the driving force causing the shrinkage, such as capillary tension, disjoining pressure, surface energy and so on. Chemical reaction and corresponding volume change known as chemical shrinkage is also considered as a reason for autogenous shrinkage.

With respect to simulation on time-dependent behaviors of concrete, a multi-scale constitutive model was developed in Concrete Lab, the University of Tokyo [1]. In this model, the driving force which principally consists of capillary tension and surface energy is simulated based on the water behaviors in micro-pores. Combining with a two-phase stiffness model, drying shrinkage could be calculated. The analytical results have been verified by tests for long time drying shrinkage. In this study, in order to obtain better predictivity of drying shrinkage at early time, and also expand the application to low w/c ratio concrete which has significant autogenous shrinkage, the authors carry out several necessary improvements based on discussion on mechanism of shrinkage. Before that, the existing model would be introduced briefly as follows.

2. MULTI-SCALE CONSTITUTIVE MODEL

2.1 Simulation of moisture state in pore-structure

The basis of this model is the pore-structure and internal moisture, which are simulated by a multi-scale system called DuCOM [1]. In this system, hydration, pore-structure and moisture transfer in hardened cement paste (hcp) are coupled and simulated synthetically. Capillary and gel porosities are calculated. Their distributions by size are described by a Raleigh-Ritz distribution function. Moisture transport and equilibrium in pore structure concerns not only water capacity and moisture gradient, but also water consumption and porosity development. Water movement is described by the following formula

$$\rho\left(\sum\phi_i\frac{\partial S_i}{\partial \mathrm{P}}\right)\frac{\partial P}{\partial t}-div(K_{tr}\nabla P)+\rho\sum S_i\frac{\partial \phi_i}{\partial t}-W_p\frac{\partial \beta_{chem.}}{\partial t}=0 \quad (1)$$

Where, i represents capillary or gel pores, and ρ is the density of water. S_i is pore saturation degree. P is pore pressure. K_{tr} is the water transport coefficients considering both liquid and vapor. β_{chem} is chemically bound water ratio and W_p is the weight of cement. Accordingly, the moisture states in hcp such as internal RH, pore pressure and saturation can be calculated.

As to water capacity in micro-pores, pore pressure difference due to capillary meniscus across the liquid-vapor interface is described by Kelvin's equation as

$$\Delta P=P_l=\frac{\rho RT}{M}\ln h \quad (2)$$

Where, ρ is the density of water, R is the gas constant and T is the absolute temperature, M is the molecular mass of water and h is the relative humidity. The pressure difference can also be obtained as

$$P_l=\frac{2\gamma}{r_c} \quad (3)$$

*1 Researcher, Dept. of Civil Engineering, University of Tokyo, Dr.E., JCI Member
*2 Associate Prof., Dept. of Civil Engineering, University of Tokyo, Dr.E., JCI Member

Where, γ is surface tension of liquid and r_c is the pore radius where the interface is present. By combining Eq. 2 and Eq. 3, the relationship between h and r_c is established by

$$\ln h = -\frac{2\gamma M}{RT\rho}\cdot\frac{1}{r_c} \tag{4}$$

As Fig. 1 shows, it is assumed that pores with radii smaller than r_c are totally filled by water. For larger pores only some are water-filled due to ink-bottle effect. The volume and surface area of ink-bottle pores are calculated based on an entrapment parameter f_r. In the pores which are not filled by condensed water, physically adsorbed water exists and is also included in the model. The saturation of gel or capillary pores can be calculated by the three portions of water by

$$S = S_{r_c} + S_{ink} + S_{ads} = \int_{r_{\min}}^{r_c} dV + \int_{r_c}^{r_{\max}} f_r dV + S_{ads} \tag{5}$$

Where, S_{rc} and S_{ink} are saturation factions in the pores smaller and larger than r_c respectively. S_{ads} is saturation fraction for adsorbed water. r_{min} and r_{max} the minimum and maximum pore radius.

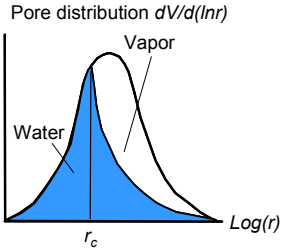

Fig. 1 Moisture distribution in micro-pores [1]

2.2 Driving force for shrinkage in hcp

Capillary tension is assumed the principal driving force at high RH. Combining the pore pressure ΔP in Eq. 2 with its effective factor β, the capillary tension is given by the following the equation

$$\sigma_{cp} = \beta\cdot\Delta P = \frac{\phi_{cp}\cdot S_{cp} + \phi_{gl}\cdot S_{gl}}{\phi_{cp} + \phi_{gl}}\cdot\Delta P \tag{6}$$

Where, σ_{cp} is volumetric stress. ϕ_{cp} and ϕ_{gl} are capillary and gel porosities. S_{cp} and S_{gl} are their saturations. β equals the average saturation.

When at low RH, physically adsorbed water starts to be lost, and surface energy changes of C-S-H gel grains becomes obvious and is assumed another driving force as

$$\sigma_{sd} = f(h)\cdot S_{pore}\cdot\gamma \tag{7}$$

Where, σ_{sd} is volumetric stress due to surface energy change. S_{pore} is surface area of gel pores, because surface energy change is thought only active in fine pores. $f(h)$ is the influence function which is related to relative humidity h according to B.E.T theory.

2.3 Two-phase composite stiffness model

Concrete is idealized as a two-phase composite consisting of hcp and aggregate. Aggregate is assumed rigid and shows elastic deformation. Shrinkage caused by aggregates is also treated in the model. Surrounding the aggregate are clusters of hcp which shows creep deformation under driving force. The details of this model can be found in the literature [1].

3. MODIFICATION ON THE EXISTING MODEL

3.1 Discrepancies in the existing model

The existing model was developed to simulate drying shrinkage of normal w/c ratio concrete and good agreement was obtained when under long time exposure, which has been shown in the past research [1]. However, if we pay attention to short time shrinkage, underestimation may be found. Fig. 2 shows the comparison with the test by Kanda et al [2]. Although the shrinkage value near 200d agrees well with test data, within tens of days the analysis provides smaller value by more than 100 micro-strains. Such a difference may lead to underestimation of cracking at the initial exposure under drying. Furthermore, the existing model is applied to autogenous shrinkage with low w/c ratio and compared with test by Tazawa et al [3], shown in Fig. 3. Shrinkage before initial setting is neglected in both the test and analysis. Obvious difference can be observed. In the tests, shrinkage increases quickly at initial days, and then the slope tends to be gentle. It has become a distinct feature that autogenous shrinkage develops rapidly at early age. However, the analysis shows continuous increase until long time. It seems that great underestimation exists at early age. Based on the discussion above, it can be concluded that discrepancies exist in the model for both autogenous and drying shrinkage, and necessary modification should be carried out to obtain better predictivity. Therefore, first the attention is paid to autogenous shrinkage.

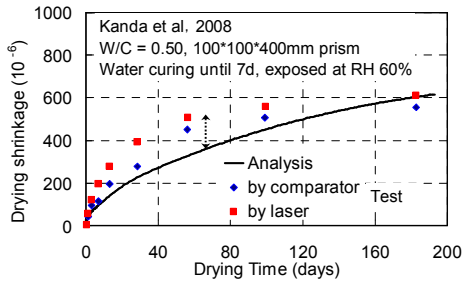

Fig. 2 Drying shrinkage by the existing model

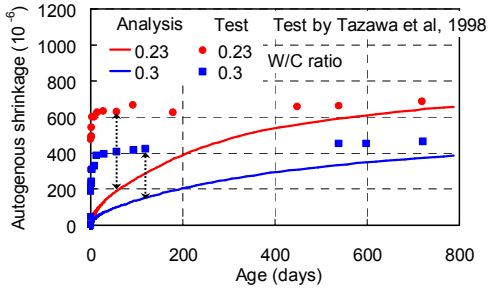

Fig. 3 Autogenous shrinkage by the existing model

3.2 The influence of chemical shrinkage on autogenous shrinkage and its simulation

Autogenous shrinkage at early age is regarded as attributed to chemical shrinkage, which is the absolute volume change of hydrates from unhydrated cement and water. When concrete is fluid, it is totally converted into macroscopic volume change. During hardening, concrete becomes rigid and a portion of chemical shrinkage can be resisted, but it still contributes to autogenous shrinkage. Therefore the role of chemical shrinkage should not be neglected. However in the existing model it is not taken into account.

The contribution of chemical shrinkage is related to the w/c ratio as reported [4]. For lower w/c, both higher chemical and autogenous shrinkages are observed. While w/c increases to normal level, chemical shrinkage still occurs but autogenous shrinkage tends to be zero. In this study, the authors attempt to explain the influence of w/c based on microscale hypothesis, as shown in Fig. 4. At the beginning, cement particles are dispersed into water and the average distance is dominated by w/c ratio. A portion of chemical shrinkage induces micro-pores while the other causes autogenous shrinkage. For high w/c, the average distance is large, so particles are independent and little interaction happens. For low w/c, distance decreases and some particles even contact each other. They tend to attract and move towards each other, resulting in more obvious macroscale volume change, i.e. autogenous shrinkage.

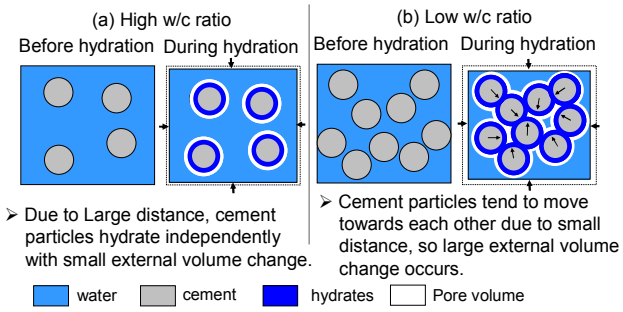

Fig. 4 Influence of w/c ratio on volume change

An equation describing autogenous shrinkage caused by chemical shrinkage is proposed as

$$\varepsilon_{ch} = v_{ch} \cdot f(\delta_m) \tag{8}$$

Where, ε_{ch} is autogenous shrinkage and v_{ch} is chemical shrinkage. δ_m is the equivalent distance of cement particles, which is calculated according to a stereological model [1]. $f(\delta_m)$ is its influence function. v_{ch} is calculated by volume change rate due to conversion from liquid to chemically bound water. $f(\delta_m)$ is given by an empirical equation. They follow the equations

$$v_{ch} = W_{ch} / (1/\rho_l - 1/\rho_{ch}) \tag{9}$$

$$f(\delta_m) = 0.045 \cdot \exp(-a \cdot \delta_m^{\ b}) \tag{10}$$

Where, W_{ch} is the weight ratio of chemically bound water. ρ_l and ρ_{ch} are densities of liquid water and chemically bound water, and the values of ρ_{ch} is assumed 1.25×10^3kg/m^3. a and b in Eq. 10 are constants with value 1.2×10^{-4} and 6.0. For normal w/c, $f(\delta_m)$ is extremely small thus can be neglected. When w/c and corresponding δ_m decreases, $f(\delta_m)$ increases and chemical shrinkage starts to affect. In the extreme case that δ_m is zero, $f(\delta_m)$ has maximum value 0.045, which implies the autogenous shrinkage value is only several percents of chemical shrinkage. Herein it has to be emphasized that the influence of chemical shrinkage on autogenous shrinkage in Eq. 8 only refers to the time after the initial setting. Before initial setting, although chemical shrinkage is totally converted into macroscopic deformation, it is not considered in the JCI test method [5], so also neglected in this model.

3.3 Simulation of capillary tension and disjoining pressure based on different pore size

With the contribution of chemical shrinkage in Eq. 8 added in Fig. 3, analytical results increase rapidly at early age and agree with test values as Fig. 5 shows. However, in the tests shrinkage increase after initial days tends to be gentle or even stagnate. High modulus may be one reason. Besides, since capillary pores are gradually filled and tend to vanish in low w/c case, sufficient driving force may not be provided. However, in Fig. 5 the analytical results increase with large slope until long time. It is suspected that the driving force at long time is overestimated in the model.

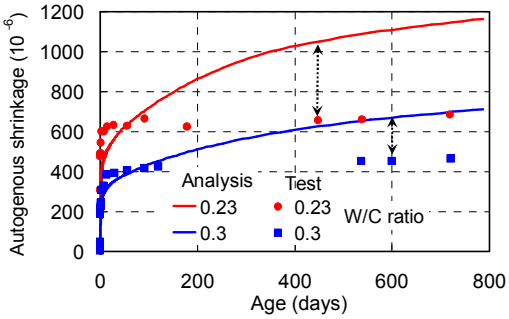

Fig. 5 Analysis with effect of chemical shrinkage

According to Eq. 6, the effective factor β is average saturation of capillary and gel pores. Therefore, in the existing model all the water is thought to contribute to capillary tension. However, micro-pore size ranges from tens of micrometers to less than nanometers. Such a large distribution may lead to varied micro-physical interaction between pores and water. Since most of capillary pores are at micrometer scale, capillary tension caused by meniscus should be the principal mechanism. On the other hand, a large portion of gel pores is at the scale of nanometers. Whether capillary tension or other mechanism dominates in those pores needs to be discussed. Beltzung et al [6] pointed out that capillary tension which occurs within the scale of nanometers is much smaller than predicted by the Laplace equation. Furthermore, as the pore size decreases to nanoscale,

due to high specific surface area and thin water film, disjoining pressure is considered more active to induce shrinkage [7, 8]. Therefore, it seems not appropriate to include all the pore-water in capillary tension in the model. Driving force caused by disjoining pressure in nanoscale pores needs to be treated separately.

In the existing model, surface energy change of gel grains is also assumed as driving force. It only becomes active when most of adsorbed water is lost and few layers of water molecules remain, which only occurs at quite low RH. However, disjoining pressure describes the behaviors of all the water in nanoscale fine pores. As long as the fine pores start to lose water, driving force arising from disjoining pressure becomes active. Therefore, the authors consider that compared with surface energy change, disjoining pressure applies more extensively in both low and mid RH. In other word, the role of surface energy in low RH can be replaced by disjoining pressure in some extent. Therefore, when disjoining pressure is adopted as one of the mechanisms in the model, the surface energy theory in Section 2.2 is no longer used.

Accordingly, the authors propose a scheme to describe the driving force as Fig. 6 shows. First, the radius r_c in Eq. 4 dominates the moisture distribution. Pores smaller than r_c are totally water-filled and others are partly filled due to inkbottle effect. Besides, another pore radius r_0 is defined to distinguish driving forces. Only in pores larger than r_0 (pores L), the internal water contributes to capillary tension. As to smaller pores (pores S), disjoining pressure is active. It acts in pores S and repulsive force occurs. r_0 is at the scale of nanometers and assumed constant 10nm. At high RH, r_c is bigger than r_0 so pores S are totally saturated. The repulsive force sustains equilibrium with the skeleton force. Driving force consists of only capillary tension in the pores L. When RH decreases and r_c becomes smaller than r_0, pores S starts to lose water and some disjoining pressures disappears. Accordingly driving force in pores S is produced due to force difference from the skeleton and causes shrinkage at low RH.

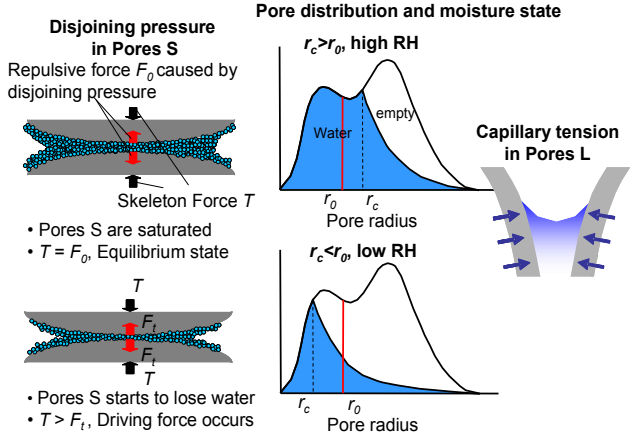

Fig. 6 Scheme of driving forces in pores with different size

Therefore, for capillary tension, the water in pores S must be excluded. Besides, compared with the average saturation in Eq. 6, the volume fraction of water seems to be a better factor, since it reflects the influence of both saturation and porosity. The capillary tension is given by

$$\sigma_{cp} = A \cdot V_L \cdot \Delta P = A \cdot (V_{cp\_L} + V_{gl\_L}) \\ = A \cdot (\phi_{cp} \cdot S_{cp\_L} + \phi_{gl} \cdot S_{gl\_L}) \quad (11)$$

Where, V_L is water volume fraction in pores L. V_{cp_L} and V_{gl_L} are the corresponding fractions in capillary and gel pores. S_{cp_L} and S_{gl_L} are saturation fractions only including water in pores L. A is influential constant with value 8.0.

As to pores S, following the discription in Fig. 6, the driving force is derived from force difference between skeleton and water, written as follows

$$\Delta F = F_0 - F_t \quad (12)$$

Where, F_0 is the force from skeleton, which equals the repulsive force when pores S are saturated. F_t is the repulsive force when some water in pores S is lost. Now the problem lies in how to calculate the repulsive force.

According to Derjaguin et al [9], the disjoining pressure between two parallel surfaces can be empirically described by

$$\Pi(h) = K \exp(-h/\lambda) \quad (13)$$

Where, K is the strength of disjoining forces, λ is the decay parameter which is in nanoscale. h is the distance between the surfaces. With the same equation Maruyama [10] derived the value in hcp as 4500 MPa by a statistical thickness-based disjoining model and shrinkage tests.

Based on Eq. 13, if pores are assumed cylinder-shaped, disjoining pressure acting on an individual pore depends on the pore size. The repulsive force should be a complex of all the disjoining pressures in various pores. Therefore, conversion from disjoining pressure to repulsive force has to be carried out. Pore size distribution, surface area and internal water information are necessary, which are simulated in DuCOM. Based on those information, the repulsive force is given by the following equation

$$F_t = \phi_s \cdot \frac{\int_{r_{\min}}^{r_0} \Pi(2r) d\chi_w}{\chi_0} \quad (14)$$

Where, ϕ_s is volume fraction of pores S. χ_0 is the total surface area of all those pores. $d\chi_w$ represents incremental of surface area due to water-filled pores with radius r. $\Pi(2r)$ is the disjoining pressure in the pores with radius r, following Eq. 13. As to the parameters K, referring to Maruyama's value, it is assumed the value as 4000MPa. λ is assumed as 10.0nm. Hence, in Eq. 14 the integral value is the force on

surface area of all the water-filled pores smaller than r_0. With the normalization by surface area the repulsive force is obtained.

When r_c is smaller than r_0, pores S are unsaturated and water can be divided into two portions. All the pores smaller than r_c are full of water, whereas in larger ones only some are water-filled due to ink-bottle effect.

Therefore, combing the entrapment parameter f_r in Eq. 5, the repulsive force in Eq. 14 can be written as the two portions

$$F_t = \phi_s \cdot \frac{\int_{r_{\min}}^{r_c} \Pi(2r)d\chi + \int_{r_c}^{r_0} f_r \cdot \Pi(2r)d\chi}{\chi_0} \tag{15}$$

Where, $d\chi$ is the incremental of surface area for all the pores with radius r.

Based on Eq. 12 and Eq. 15, the driving force in the form of stress can be finally written as

$$\sigma_{gl} = F_0 - F_t = \phi_s \cdot \frac{\int_{r_{\min}}^{r_0} \Pi(2r)d\chi}{\chi_0} - \phi_s \cdot \frac{\int_{r_{\min}}^{r_c} \Pi(2r)d\chi + \int_{r_c}^{r_0} f_r \cdot \Pi(2r)d\chi}{\chi_0} \tag{16}$$

$$= \phi_s \cdot \frac{\int_{r_c}^{r_0} \Pi(2r)d\chi - \int_{r_c}^{r_0} f_r \cdot \Pi(2r)d\chi}{\chi_0}$$

Combining with capillary tension in Eq. 11, the total driving force is obtained as follows

$$\sigma = \sigma_{cp} + \sigma_{gl} \tag{17}$$

4. SIMULATION of AUTOGENOUS AND DRYING SHRINKAGE

With the improvement on the driving force, autogenous shrinkage shown in Fig. 5 is simulated again. As Fig. 7 shows, it can be found that by the improved model the analysis well reflects the shrinkage development until long time. During the initial days, shrinkage develops rapidly to hundreds of microstrains. Besides, the slope after early age is also alleviated, resulting in slow increase for long time. The improvement lies in the exclusion of nano-scale pores from capillary tension discussed above. In low w/c case, most of capillary pores are filled by hydrates and fine pores occupy the main portion. Accordingly disjoining pressure rather than capillary tension dominates the driving force, which is mainly active at relatively lower RH than the condition by self-desiccation. Besides, compared with Eq. 6, the new formula of capillary tension in Eq. 11 adopts the water volume fraction as the influential factor rather than saturation. For low w/c ratio it is more reasonable, since little water volume exist in capillary pores even if the saturation is not low.

Furthermore, the improved model is used for drying shrinkage. First of all, the case in Fig. 2 is calculated again by the improved model and shown in Fig. 8. The drying shrinkage within tens of days is much increased from the original model, while the shrinkage development afterwards becomes slower, giving better agreement with test data. This is also because the subdivision of driving forces. For w/c ratio 0.5 at RH 60%, a large portion of drying force is derived from capillary tension, which acts principally at early time of drying. Therefore as the hydration goes on the increase of driving force becomes slow and less shrinkage increment is observed at long time.

Besides, the shrinkages behaviors under drying condition with various w/c ratios are simulated based on both the original and improved models. The results are compared with test by Kiyohara et al [11]. In the test, concrete with varied w/c ratio from 0.25 to 0.65 were exposed at RH 60% after 7d curing and shrinkage are measured. All the specimens in the tests are prisms with size 100mm×100mm ×400mm. In the analysis as an influential factor, the shrinkage of aggregate is also taken into account so that within 1 year around 400 micro-strains of shrinkage is caused by aggregate. The final comparison is shown in Fig. 9. Obviously the original model can not be applied to low w/c ratio. In the analysis by the original model, the shrinkage with w/c ratios 0.25 and 0.35 become much larger than the test data. On the other hand, with the improved model, the influence of w/c ratio on shrinkage can be reflected and well agree with test. Higher w/c ratio will induce higher shrinkage, shown both in test and the improved model. As to the precision on normal w/c ratio such as 0.55, the shrinkage at early drying time is also improved in the value, although still some underestimation exists. For the gap between analysis and test at early drying time, more comprehensive investigation needs to be conducted in the future in order to obtain better prediction accuracy.

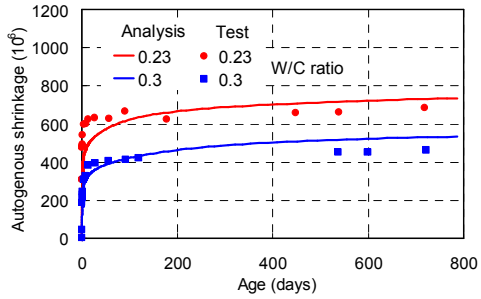

Fig. 7 Autogenous shrinkage by the improved model

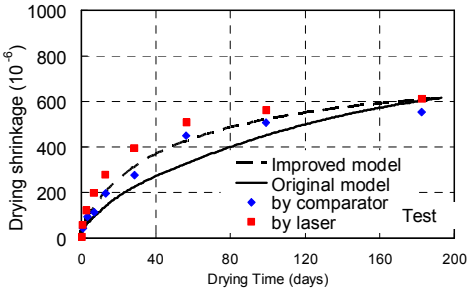

Fig. 8 Drying shrinkage by the improved model

Finally, the improved model is applied to the drying shrinkage under varied relative humilities and

compared with test by Tazawa et al [3]. In the test concrete with w/c ratio 0.5 were exposed under RH 40%, 60%, 80%, 90% after 7d sealed and compared the drying shrinkage with sealed case. The size of specimens is 100mm×100mm×400mm. As Fig. 10 shows, the improved model can well simulate the shrinkage development. As RH decreases drying shrinkage increases.

The above verifications by shrinkage indicates that with the combination of both capillary tension and disjoining pressure in the improved model, sufficient driving force can be supplied under varied drying conditions. Therefore, it can be concluded that the modification in this study is reasonable.

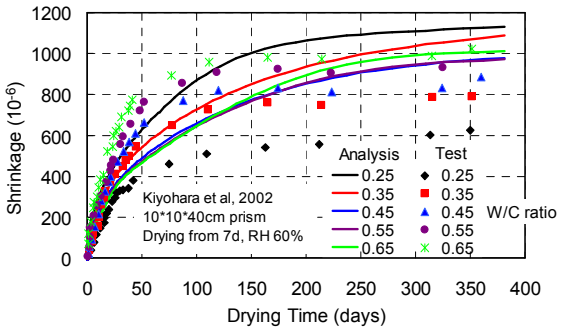

(a) By the original model

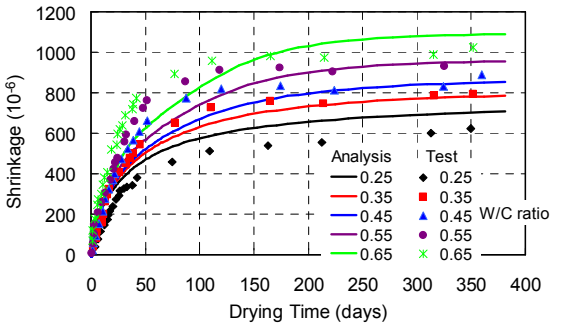

(b) By the improved model

Fig. 9 shrinkage behavior under dying condition with varied w/c ratios

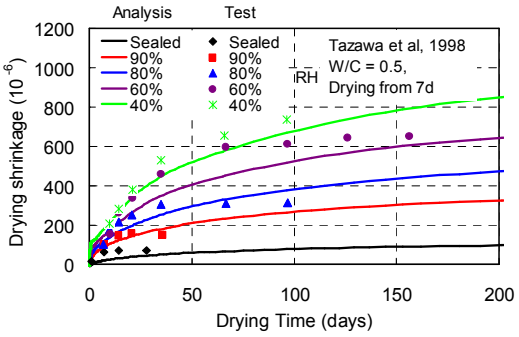

Fig. 10 Drying shrinkage with varied RH by the improve model

5. CONCLUSION

Several mechanisms can be used to explain and simulate autogenous and drying shrinkage of concrete. In the improved model a combination of chemical shrinkage, capillary tension and disjoining pressure is adopted as the driving mechanism. They are considered acting at different stages or in different micro-pores. At initial days, chemical shrinkage contributes significantly to autogenous shrinkage, while capillary tension and disjoining pressure act principally for drying shrinkage and long time autogenous shrinkage. The role of these driving forces can be described by the improved model from micro-scale. Verification by experiment of both autogenous and drying shrinkage shows the rationality of the improvement.

REFERENCES

[1] Maekawa, K., Ishida, T. and Kishi, T., "Multi-scale Modeling of Structural Concrete," Taylor & Francis, 2008

[2] Kanda, T. et al., "An experimental study for simplified drying shrinkage testing method," J. Struct. Constr. Eng., AIJ, Vol.73, No.628, 2008, pp. 851-857. (In Japanese)

[3] Tazawa, E. and Miyazawa, S., "Effect of constituents and curing condition on autogenous shrinkage concrete," Proceedings of the International Workshop, Hiroshima, 1998, pp. 269-280.

[4] Holt, E., "Contribution of mixture design to chemical and autogenous shrinkage of concrete at early ages," Cement and Concrete Research, Vol.35, 2005, pp. 464-472.

[5] Japan Concrete Institute, "Test method for autogenous shrinkage and autogenous expansion of cement paste, mortar and concrete," Report by Technical Committee on Autogenous Shrinkage of Concrete, 1996, pp195-198. (In Japanese)

[6] Beltzung, F. and Wittmann, F.H., "Role of disjoining pressure in cement based materials," Cement and Concrete Research, Vol.35, 2005, pp. 2364-2370.

[7] Espinosa, R. M. and Franke, L., "Influence of the age and drying process on pore structure and sorption isotherms of hardened cement paste," Cement and Concrete Research, Vol.36, 2006, pp. 1969-1984.

[8] Powers, T. C. "Mechanism of shrinkage and reversible creep of hardened cement paste," Proceedings of International Conference on the Structure of Concrete, London, 1968, pp. 319-344.

[9] Derjaguin, B. V. and Churaev, N. V., "Properties of water layers adjacent to interfaces, " in "Fluid Interfacial Phenomena," John Wiley & Sons Ltd, 1985, pp. 663-738.

[10] Maruyama, I., "Origin of drying shrinkage of hardened cement paste: hydration pressure," Journal of Advanced Concrete Technology, Vol.8, 2010, pp. 187-200.

[11] Kiyohara, C. et al., " Equation for predicting drying shrinkage strain of concrete based on the theory of composite material," Summaries of Technical Papers of Annual Meeting, AIJ, Hokuriku, 2002, pp. 555-556. (In Japanese)